1606 *Biochemistry* **2010,** *49,* 1606–1615
DOI: 10.1021/bi901798g

BIOCHEMISTRY
including biophysical chemistry & molecular biology
Article

Nuclear Magnetic Resonance Study of the Role of M42 in the Solution Dynamics of *Escherichia coli* Dihydrofolate Reductase[†]

Randall V. Mauldin[‡] and Andrew L. Lee*[,‡,§]

[‡]*Department of Biochemistry and Biophysics, School of Medicine and* [§]*Division of Medicinal Chemistry and Natural Products, Eshelman School of Pharmacy, University of North Carolina, Chapel Hill, North Carolina 27599*

Received October 20, 2009; Revised Manuscript Received January 14, 2010

ABSTRACT: It is widely recognized that key positions throughout a protein's structure contribute unequally to function. In light of recent studies that suggest protein dynamics are required for function, a number of these residues may serve to promote motions required for ligand binding and catalysis. In this nuclear magnetic resonance (NMR) study, the conformational dynamics of the dihydrofolate reductase (DHFR) mutant M42W, in the presence of methotrexate and NADPH, are characterized and compared to those of the wild-type enzyme. M42 is distal to the active site, yet the M42W substitution regulates catalysis and ligand affinity and is therefore analogous to an allosteric modulator of DHFR function. To gain understanding of how this mutation regulates activity, we employ a "pandynamic" strategy by measuring conformational fluctuations of backbone amide and side-chain methyl groups on multiple time scales. Changes in pico- to nanosecond dynamics indicate that the mutational effects are propagated throughout a network of interacting residues within DHFR, consistent with a role for M42 as a dynamic communication hub. On the micro- to millisecond time scale, mutation increases the rate of switching in the catalytic core. Mutation also introduces switching in the adenosine binding subdomain that occurs at a higher frequency than in the catalytic core and which correlates with the rate of product release for M42W-DHFR. Finally, a structurally inferred analysis of side-chain dynamics suggests that the M42W mutation dampens motional contributions from nonlocal sources. These data show that the M42W mutation alters the dynamics of DHFR and are consistent with theoretical analysis that suggests this mutation disrupts motion that promotes catalysis.

Conformational dynamics are intimately linked to highly evolved processes such as ligand binding, catalysis, and product release (*1*−*4*). Therefore, it is likely that conserved amino acids contribute to these motions on multiple time scales (*5*−*7*). To test this hypothesis, we have systematically examined the dynamics of *Escherichia coli* dihydrofolate reductase (DHFR)[1] M42W (methionine 42 to tryptophan mutant) using state-of-the-art nuclear magnetic resonance (NMR) spin relaxation techniques. M42 is highly conserved among bacterial DHFRs, and amino acid substitutions at position 42 alter every aspect of the catalytic cycle (*8*−*11*).

DHFR has long served as a model system for examining the relationships among enzyme sequence, structure, and function (for a review, see ref *12*). DHFR catalyzes the NADPH-dependent reduction of 7,8-dihydrofolate to 5,6,7,8-tetrahydrofolate, a metabolic precursor of purine bases and certain amino acids. It is a monomeric enzyme composed of 159 amino acids that can be divided into two subdomains: the adenosine binding domain and the loops domain (Figure 1A) (*13*). Structural analysis indicates DHFR cycles between two distinct, ligand-dependent structural states termed "closed" and "occluded" in reference to the conformation of the Met20 loop (*13*). In the closed conformation, the substrate and cofactor are positioned within the active site poised for catalysis, whereas in the occluded conformation, the Met20 loop blocks the access of the cofactor to the reactive center. The rate of exchange between these conformational states correlates with the rate of catalysis and product release, suggesting a dynamic mechanism for enzyme function (*3*, *13*).

One of the most interesting and well-known features of DHFR is that its kinetics can be modulated by distal mutations, such as M42W (*8*, *9*). As shown in Figure 1A, M42 is located in the hydrophobic core of the adenosine binding subdomain, approximately 10 Å from the reactive center and 14 Å from the "catalytic residue", D27. M42W drastically decreases the rate of hydride transfer and increases the rate of product dissociation, making chemistry the rate-limiting step of catalysis (*8*). Furthermore, the mutation introduces a catalytically significant structural prearrangement step into the reaction cycle (*8*). Thus, M42W can be considered a long-range effector, analogous to an allosteric regulator of DHFR catalysis.

If dynamical fluctuations are required for enzyme catalysis, it is to be expected that kinetically significant mutations modulate these motions (*2*, *14*). Molecular dynamics simulations of M42W-DHFR

[†]This work was funded by National Institutes of Health Grant GM083059 (to A.L.L.).

*To whom correspondence should be addressed: University of North Carolina, Division of Medicinal Chemistry and Natural Products, Eshelman School of Pharmacy, Beard Hall, CB# 7568, Chapel Hill, NC 27599-7568. E-mail: drewlee@unc.edu. Phone: (919) 966-7821. Fax: (919) 843-5150.

[1]Abbreviations: AIC, Akaike information criteria; BIC, Bayesian information criteria; CPMG, Carr−Purcell−Meiboom−Gill; DHFR, dihydrofolate reductase; M42W, methionine 42 to tryptophan mutation; MTX, methotrexate; NADPH, nicotinamide adenine dinucleotide phosphate; NMR, nuclear magnetic resonance; NOE, nuclear Overhauser enhancement; pABG, (*p*-aminobenzoyl)glutamate; PDB, Protein Data Bank; R_1, spin−lattice (longitudinal) relaxation; R_2, spin−spin (transverse) relaxation; RDCs, residual dipolar couplings; S^2, generalized order parameter; $S_{axis}{}^2$, order parameter of the methyl symmetry axis; τ_e, effective correlation time; $\tau_{e,axis}$, effective correlation time of the methyl symmetry axis; TMP, trimethoprim; WT, wild type.

 Published on Web 01/14/2010

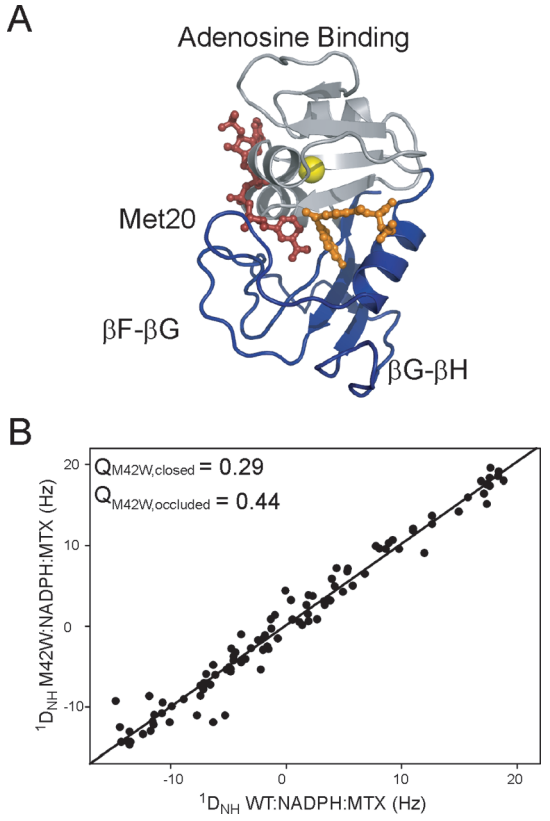

FIGURE 1: M42W-DHFR in complex with NADPH and MTX adopts the catalytic closed conformation. (A) The structure of DHFR in complex with MTX (orange) and NADPH (yellow) is shown in the closed conformation. The yellow sphere indicates M42, and the functional loops are labeled. DHFR is a single-domain protein that can be divided into two subdomains: the adensosine binding domain (gray) and the loops domain (blue). (B) Residual dipolar couplings indicate M42W-DHFR is in the closed conformation. Wild-type and M42W E−NADPH−MTX dipolar couplings are plotted. The *Q* factors for the closed (PDB entry 1rx3) and occluded (PDB entry 1rx5) complexes are shown in the correlation plot.

indicate the dynamics within the closed conformation are indeed altered (*15*). Specifically, the mutation disrupts a network of coordinated motion that promotes hydride transfer (*16*). Unfortunately, the exact mechanism by which the distal perturbation is transferred to the active site remains unknown, and experimental data related to this problem are sparse.

We have previously shown that perturbation within the active site of DHFR is propagated to distal regions of the protein, including the adenosine binding subdomain that contains M42 (*17*). In that study, we reported the subnanosecond and micro- to millisecond dynamics of DHFR in response to binding the drugs methotrexate (MTX) or trimethoprim (TMP) to the wild-type holoenzyme (WT−NADPH). Changes in NMR-derived backbone and side-chain pico- to nanosecond order parameters indicated that long-range dynamics are influenced by ligand binding (*17*). Concurrently, conformational switching on the micro- to millisecond time scale is quenched by drug binding. In essence, the conformational dynamics within the closed ground state and the transition into higher-energy states are controlled by molecular interactions within the active site (*17*).

In this report, we turn our attention to changes in DHFR dynamics related to the M42W mutation. While other mutations at this site such as M42F alter the rate of catalysis (k_{off}), the M42W substitution is the only mutation that alters the rate of hydride transfer (*8*, *9*). Thus, this model system provides a unique opportunity to study the dynamics that may lead to a decrease in the rate of chemistry. Using NMR spin relaxation methods, we examine the pico- to nanosecond and micro- to millisecond dynamics of M42W-DHFR in complex with NADPH and MTX, using both backbone and side chain groups as probes. This "pandynamic" approach takes full advantage of the excellent sensitivity of NMR spectroscopy to molecular motion on different time scales and for different types of atomic groups. Comparison to the wild-type ternary complex provides a detailed map of changes in motion due to mutation. Furthermore, because the ternary MTX complex is a mimic for the transition state (*13*), the observed dynamic changes may be particularly relevant to catalysis. We find that the mutation modulates backbone and side-chain dynamics within the adenosine binding domain but also in the active site and loops domain. We also present an analysis that suggests M42W attenuates nonlocal influence on the pico- to nanosecond dynamics of the enzyme. Finally, the mutation changes the rate of micro- to millisecond conformational switching within the catalytic core and introduces an additional slow motional mode on the same time scale as product release observed in the M42W enzyme. Taken together, these results suggest that M42 acts as a dynamic hub, connecting the loops and adenosine binding subdomains, and that manipulation of these interactions may modulate function. Our data support the hypothesis that M42W changes the rate of hydride transfer and product release by modulating DHFR's highly evolved conformational fluctuations (*10*, *17*−*19*).

MATERIALS AND METHODS

Protein Purification and NMR Sample Preparation. The M42W mutation was performed using the QuickChange mutagenesis protocol (Stratagene). Plasmid DNA was sequenced at the University of North Carolina Genomic Analysis Facility. Either isotopically labeled M42W-DHFR was expressed and purified using the same protocol that was used for the wild-type protein discussed elsewhere (*17*). ^{15}N-labeled protein (no deuteration) was used for the CPMG relaxation dispersion experiments. The concentration of M42W-DHFR was assayed spectrophotometrically [ε_{280} = 34100 M^{-1} cm^{-1} (*9*)].

All NMR experiments were performed on 1 mM protein samples in buffer containing 70 mM HEPES (pH 7.6), 20 mM KCl, 1 mM EDTA, 1 mM DTT, 20 mM NADPH, 3−5 mM MTX, 20 mM glucose 6-phosphate, and 10 units of glucose-6-phosphate dehydrogenase. The concentrations of NADPH and MTX were determined spectrophotometrically using published extinction coefficients (*20*). The protein samples were placed in an amber NMR tube and flame-sealed under argon.

NMR Experiments. All NMR experiments were performed at 298 K (calibrated with neat methanol) on Varian INOVA spectrometers. Backbone C^{β}, C^{α}, N, and H chemical shifts for non-proline residues were assigned using gradient-enhanced HNCACB, CBCA(CO)NH, and HNCA experiments conducted at 500 MHz (*21*). Side chain methyl resonances were assigned using the three-dimensional (3D) $HCCH_3$-TOCSY experiment (*22*). Methionine resonances were assigned on the basis of the wild-type chemical shifts (*17*). NMR data were processed using NMRPipe and analyzed using NMRDraw (*23*) and NMRView (*24*). PINE aided in backbone resonance assignment (*25*).

Relaxation dispersion measurements were conducted using ^{15}N CPMG-based relaxation dispersion pulse sequences (*26*) on 500 and 700 MHz spectrometers equipped with cryogenic probes.

Fifteen relaxation time points, including two duplicate planes, were collected at CPMG field strengths ($1/\tau$) ranging from 100 to 1800 s^{-1}. A reference experiment omitting the 40 ms constant time relaxation period was also collected for calculation of the effective R^2 values (*27*).

Standard backbone ^{15}N R_1, R_2, and $\{^1H\}-^{15}N$ NOE (*28*) and side chain D_z and D_y (*29*) relaxation spectra were acquired as described previously (*17*). Backbone relaxation was performed at 500 and 600 MHz, whereas side chain relaxation experiments were performed at 600 and 700 MHz.

Residual Dipolar Coupling Analysis. Residual dipolar couplings were measured using the two-dimensional (2D) IPAP-HSQC experiment at 500 MHz (*30*). M42W-DHFR was aligned using a stretched acrylamide gel (*31*) as described previously (*17*). Peak positions in the IPAP-HSQC experiment were extracted using the NMRPipe modules ipap.tcl and nlinLS (*23*). Dipolar coupling values were calculated by subtracting the isotropic and anisotropic coupling values. Quality factors (Q) were calculated using REDCAT (*32*). All residues for which RDCs could be calculated were included in Q calculations, except position 22, which typically is in large disagreement with the crystal structures used.

Lipari−Szabo Model-Free Analysis. Picosecond to nanosecond backbone amide and side chain methyl dynamics were characterized using the Lipari−Szabo model-free formalism (*33*). Consistent with wild-type DHFR, the isotropic rotational correlation time for M42W-DHFR is 10.2 ns. Rotational anisotropy was calculated using the local D_i method (*34*) using the DHFR structure 1rx3. The backbone relaxation data were fit using an anisotropic correction ($D_{\|}/D_{\perp} = 1.14$) to minimize model selection error (*35*). Backbone relaxation data were best fit to the five model-free models using the in-house program relxn2.2 assuming a 1.02 Å $^1H-^{15}N$ bond distance and a −170 ppm ^{15}N chemical shift anisotropy. The correct model was selected using Akaike's information criterion (*36*). Side chain model-free parameters were best fit using relxn2.2 assuming a quadrapolar coupling constant of 165 kHz.

Relaxation Dispersion Analysis. Conformational exchange on the micro- to millisecond time scale results in a change in $R_{2,eff}$ as a function of τ_{cp}. Only residues that display an overall change in $R_{2,eff}$ greater than 2 s^{-1} were analyzed. Relaxation dispersion data were best fit to models assuming no conformational exchange ($R_{2,eff} = R_2^0$) and a simple two-state model. A statistical F test was used to identify residues that exhibit chemical exchange (α critical = 0.01). Residues that did not pass the F test were removed from the data set. As previously described by our group and others, residues 129−134 and 155−159 in DHFR report on ligand-independent conformational exchange (*3*, *17*, *37*). These residues were not considered in any global fit reported here. The effective R_2 rates as a function of τ_{cp}^{-1} were best fitted to the Carver−Richards equation for two-state exchange (*38*) using the in-house program exrate2.0, as described previously (*17*). The Bayesian information criterion (*36*) was used to group values for global fitting.

Statistical Hypothesis Testing and Comparison with Calculated Order Parameters. Fisher's exact test was used for contingency table analysis (*39*). The p value was calculated using the fisher.test routine implemented in R version 2.7.1 (http://www.r-project.org).

S_{model}^2 values were calculated using the online server (http://spinportal.magnet.fsu.edu/methylside chains2/methylside chains2.html) provided by Brüschweiler and co-workers (*40*) using crystal structure 1rx3 (WT−NADPH−MTX). Calculations performed using structures 1rx1 (WT−NADPH) and 1rx2 (WT−$NADP^+$−folate) resulted in nearly identical results (data not shown). Correlation coefficients were calculated using Excel 2003 (Microsoft Inc.). Fisher's r to z transform (eqs 1 and 2) was used to compare two correlation coefficients.

$$r' = 0.5 \log_e \left| \frac{1+r}{1-r} \right| \quad (1)$$

$$z = \frac{r_1' - r_2'}{\sqrt{\frac{1}{n_1 - 3} - \frac{1}{n_2 - 3}}} \quad (2)$$

In this case, we were interested in testing the hypothesis H_0: $r_1 = r_2$, H_a: $r_1 > r_2$. Therefore, a one-tailed p value is appropriate and was calculated from the derived z score using the R function pnorm.

RESULTS

The Ternary M42W-DHFR Complex Adopts the Closed Conformation in Solution. As shown in Figure 1A, methionine 42 is located in the hydrophobic core of the protein and is highly conserved among bacterial DHFRs (*19*, *41*). The van der Waals volume of the tryptophan side chain is ~30 $Å^3$ larger than that of methionine, making it pertinent for the examination of the structural consequences of M42W. Backbone residual dipolar couplings are a powerful tool for assessing structural perturbations caused by point mutations (*42*). The mutant and wild-type RDCs are linearly correlated ($R^2 = 0.96$), indicating very little if any structural rearrangement occurs upon mutation (Figure 1B). The "quality factor" Q presented by Bax and co-workers (*43*) provides a metric for comparing the experimental RDCs to the crystal structures for closed and occluded DHFR (PDB entries 1rx3 and 1rx5, respectively). The results indicate the overall structure of M42W-DHFR is similar to the closed crystal structure ($Q = 0.29$). By comparison, $Q = 0.44$ when the experimental data are compared to a model of the occluded structure.

The possibility remains that the low Q value obtained for the closed model does not reflect the actual level of structural rearrangement around the point of mutation. One could easily envision a situation in which structural perturbation within the adenosine binding subdomain is masked in the global Q value by strong agreement in the loops subdomain. To examine this scenario, the RDCs were separated into two groups: residues in the adenosine binding subdomain (38−107) and loops domain (1−37 and 108−159) (*13*). Q values were calculated for both subdomains using the same alignment tensor. It should be mentioned that the alignment tensor does not significantly change if we consider the adenosine binding and loops subdomains as individual bodies (data not shown). We find that the Q value for the adenosine binding subdomain agrees very well with that of the crystal structure ($Q = 0.25$). Furthermore, the agreement is better for the adenosine binding subdomain than for the loops subdomain ($Q = 0.33$). From this analysis, we can conclude the backbone structure of DHFR is generally not perturbed by the M42W mutation.

Lipari−Szabo Analysis of Backbone Picosecond to Nanosecond Dynamics. The backbone dynamics of the ternary M42W complex were measured using ^{15}N R_1, R_2, and $\{^1H\}-^{15}N$

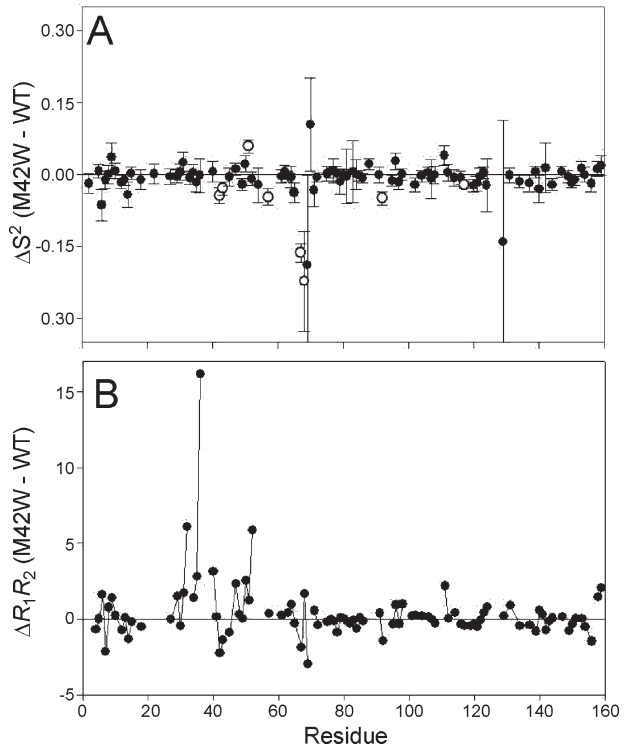

FIGURE 2: Changes in backbone dynamics indicate pico- to nanosecond and micro- to millisecond dynamical perturbation. (A) Changes in the backbone order parameter as a result of the M42W mutation are plotted. Residues that exhibit a significant change in order parameter are indicated by the empty circles. (B) R_1R_2 is sensitive to exchange on the micro- to millisecond time scale. The differences in R_1R_2 between the M42W and wild-type DHFR−NADPH−MTX complexes are plotted. Residues with an increased level of conformational exchange are indicated by increased ΔR_1R_2 values.

steady state NOE parameters (*28*) at ^{1}H spectrometer frequencies of 500 and 600 MHz. The relaxation data were interpreted using the Lipari−Szabo model-free formalism, which yields a generalized order parameter (S^2) and internal correlation time (τ_e) for each residue (*33*). The S^2 can range from 0 to 1, indicating completely isotropic to fixed dynamics of the bond vector, respectively. Model-free parameters were calculated for 112 of the 148 non-proline residues in M42W-DHFR. AIC statistics (*36*) were used to identify residues that require an additional term (R_{ex}) to compensate for elevated R_2 rates due to conformational exchange (micro- to millisecond dynamics) or an extended model that accounts for slower nanosecond motion requiring a fast (S_f^2) and slow (S_s^2) order parameter (model 5) (*44*). These results are summarized in Figure 2A and Table S1 of the Supporting Information. M42W increases the number of residues that require R_{ex} to fit the data: 26 compared to 12 in the wild-type MTX ternary complex (*17*). The presence of increased slower motion (micro- to millisecond) is confirmed by inspection of the outliers in an R_1R_2 plot (*45*). As shown in Figure 2B, residues between positions 32 and 40 and between positions 46 and 50 generally have elevated R_1R_2 values compared to that of the wild type. Most of the backbone relaxation is satisfactorily described by model-free parametrization with the exception of K32, L36, D37, and E129. In each case, model 5 (S_f^2, S_s^2, and τ_e) was statistically selected, but the obvious presence of elevated R_2 rates precluded reliable fits of the data. Therefore, we conclude the motion in these regions is complex and cannot be satisfactorily described by a Lipari−Szabo model-free model.

As shown in Figure 2A, the average difference between mutant and wild-type backbone order parameters is near zero, indicating the mutation does not drastically alter the overall pico- to nanosecond backbone dynamics of DHFR. Residues W42, G43, G51, R57, G67, T68, V92, and A117 display differences that are greater than or equal to twice the experimental error (≥95% confidence interval) and therefore exhibit significant changes in backbone motion. It is intriguing to note that residues G67 and T68 located in the adenosine binding loop, which exhibit the largest change in backbone dynamics, are ~15 Å (Cα to Cα) from M42. Residues 67−69 show slight dynamic response to binding of MTX to the wild-type holoenzyme (*17*), and mutation within the adenosine binding loop alters the rate of catalysis (*46*). Thus, the data suggest that M42 is part of a dynamic network of interactions that link the active site to the adenosine binding loop (*46*−*48*).

Picosecond to Nanosecond Side Chain Methyl Dynamics. The dynamics of methyl-containing side chains were quantified using deuterium-based relaxation methods. The D_z and D_y relaxation rates (*29*) were measured at ^{1}H spectrometer frequencies of 600 and 700 MHz. Analogous to the backbone dynamics measurements, the side chain order parameter, S_{axis}^2, reports on the rigidity of the methyl symmetry axis (*49*). Reliable order parameters were obtained for every resolved resonance except residues 54 and 110. For both of these residues, the resonances were extremely broad, indicative of conformational exchange. The results are summarized in Figure 3 and Table S2 of the Supporting Information.

To evaluate the magnitude of perturbation that results from the M42W mutation, changes in methyl S_{axis}^2 were calculated [$\Delta S_{axis}^2 = S_{axis(M42W)}^2 - S_{axis(WT)}^2$]. As with the backbone ΔS^2 analysis, significant changes were identified as absolute ΔS_{axis}^2 values equal to or greater than twice the propagated error. Methyl groups L4$^{\delta1}$, L4$^{\delta2}$, L8$^{\delta2}$, M16$^{\varepsilon}$, A19$^{\beta}$, M20$^{\varepsilon}$, I61$^{\delta1}$, T73$^{\gamma2}$, I82$^{\delta1}$, I82$^{\gamma2}$, I91$^{\gamma2}$, I115$^{\delta1}$, and A145$^{\beta}$ become more rigid and L28$^{\delta1}$, I41$^{\delta1}$, I60$^{\delta1}$, L62$^{\delta1}$, L62$^{\delta2}$, and I94$^{\delta1}$ more flexible upon mutation (Figure 3A). The largest change in S_{axis}^2 occurs at I94$^{\delta1}$ ($\Delta S_{axis}^2 = -0.3$) which is located within the active site of DHFR. The average ΔS_{axis}^2 is near zero, indicating the overall conformational entropy does not change as a result of the mutation. The internal correlation time ($\tau_{e,axis}$) is robustly defined in the analysis of side-chain relaxation data and can be interpreted as a change in the dynamic character of the amino acid (*1*, *50*). As shown in Figure 3B, methyl groups L8$^{\delta1}$, A26$^{\beta}$, V72$^{\gamma1}$, I94$^{\gamma2}$, and V99$^{\gamma2}$ exhibit statistically significant $\Delta\tau_{e,axis}$ values.

M42W elicits a long-range dynamic response within DHFR. As shown in Figure 4A, significant ΔS_{axis}^2 values cannot be rationalized by distance with respect the mutation alone, although a general trend of a larger perturbation at a shorter distance does exist. For example, while I94$^{\delta1}$ is < 5 Å from M42 ($\Delta S_{axis}^2 = -0.3 \pm 0.06$), A145$^{\beta}$ is 30 Å from the site of mutation and becomes more rigid by 0.092 ± 0.026. In the same light, I50$^{\delta1}$ ($\Delta S_{axis}^2 = -0.03 \pm 0.03$) does not significantly change in spite of being proximal (< 5 Å) to the point of mutation. Furthermore, the dynamical change does not correlate with the change in methyl chemical shift (Figure 4B) (*51*). On an individual basis, as with distance from the point of mutation, chemical shift change is not a reliable predictor of ΔS_{axis}^2. These results are not altogether surprising because distance and chemical shift change are largely dependent on structural factors within the protein. S_{axis}^2 values report only on the dynamics at a particular methyl group (*49*). Moreover, the data suggest that dynamic changes can be

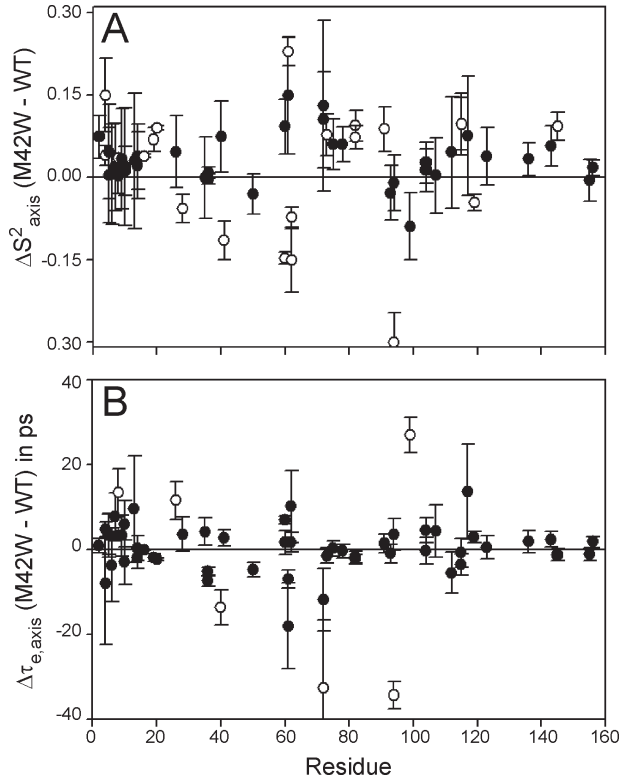

FIGURE 3: Changes in side chain methyl dynamics indicate widespread perturbation. (A) Changes in the amplitude of pico- to nanosecond side chain dynamics (ΔS_{axis}^2) are plotted. Residues that experience significant dynamical perturbation are indicated by the empty circles. (B) The internal correlation time for side chain methyl groups is robustly defined and can be interpreted as a change in dynamics. The empty circles indicate residues that change two times the propagated error and greater than 10 ps.

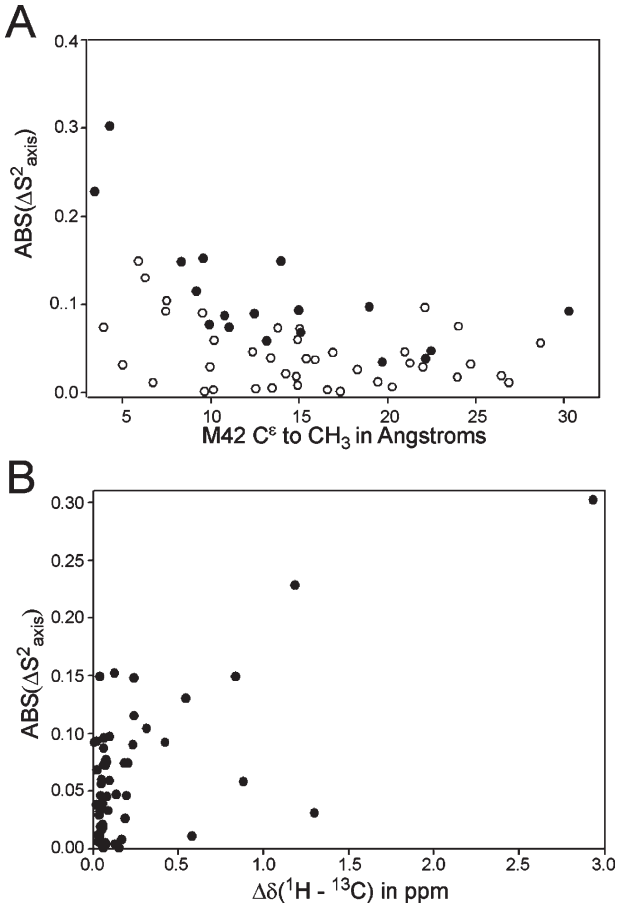

FIGURE 4: Dynamical perturbations as a result of the M42W mutation are largely independent of distance from the mutation and structural perturbation. (A) The absolute changes in S_{axis}^2 as a function of distance from the mutation are plotted. Filled circles indicate significant changes in pico- to nanosecond methyl dynamics (see Figure 3). (B) The change in S_{axis}^2 does not correlate with the change in methyl chemical shift upon mutation. Structural perturbation is necessarily a prerequisite for dynamical perturbation. The change in methyl chemical shift was calculated using a Euclidean distance (*61*).

propagated in the absence of structural perturbation, supporting a dynamic mechanism for intramolecular communication or allostery without structural change (*51*−*54*).

Microsecond to Millisecond Conformational Switching in the M42W-DHFR Ternary Complex: Introduction of New Motion. The micro- to millisecond conformational dynamics of M42W-DHFR were measured using relaxation-compensated CPMG experiments (*26*). Whereas Lipari−Szabo model-free analysis typically probes the internal dynamics within a single conformational basin, relaxation dispersion quantifies the exchange between two or more distinct conformations (*38*). The change in R_2 as a function of CPMG field strength (τ_{cp}^{-1}) is sensitive to the exchange rate ($k_{ex} = k_1 + k_{-1}$), a change in chemical shift between conformations ($\Delta\omega$), and the population of each state (p_a or p_b) (*38*). Often, relaxation dispersion data are fitted to a single "global" exchange rate and population (*27*). This assumption is justified since it is unlikely that two residues in the same region of the protein move at a vastly different rate as they are likely reporting on the same exchange event.

In M42W-DHFR bound to NADPH and MTX, 20 residues exhibit a significant change in R_2 as a function of τ_{cp}. As shown in Figure 5, micro- to millisecond exchange clusters in two main regions: the catalytic core of the protein (L8, A9, V10, R12, I14, W22, A29, W30, F31, K32, R33, N34, L104, Y111, and L112) and residues in the adenosine binding domain located "above" the (*p*-aminobenzoyl)glutamate (pABG) binding cleft (V40, T46, I50, R52, and L54) (*13*). The number of residues that display measurable conformational exchange in the M42W−NADPH−MTX complex is twice that of the wild-type ternary drug complex at 298 K (*17*). Clearly, M42W alters the pattern of resonances that experience R_2 relaxation dispersion, or motion on the time scale of catalysis and ligand binding.

It should be noted that the equilibrium dissociation constants for both NADPH and folate ligands are unaltered in the closed conformation of M42W-DHFR (*8*). For the wild-type protein, the dissociation constants for NADPH and dihydrofolate are 0.34 and 0.33 μM, respectively (*8*, *20*). By comparison, the equilibrium dissociation constants for M42W for NADPH and dihydrofolate are 0.27 and 0.43 μM, respectively, and MTX binds several orders of magnitude tighter (*8*). Relaxation dispersion experiments require that the excited state be populated between 1 and 5% in solution. Given the experimental conditions (20-fold excess of NADPH and 3−5-fold excess of MTX), ligand exchange is an unlikely source of line broadening in the relaxation dispersion experiments. Thus, the most likely source of R_2 dispersion is protein motion or ligand fluctuation within the active site.

The best fit exchange rates for individual dispersion curves cluster into two groups: one group characterized by rates ranging from 1000 to 2000 s^{-1} and one with rates ranging from 3000 to

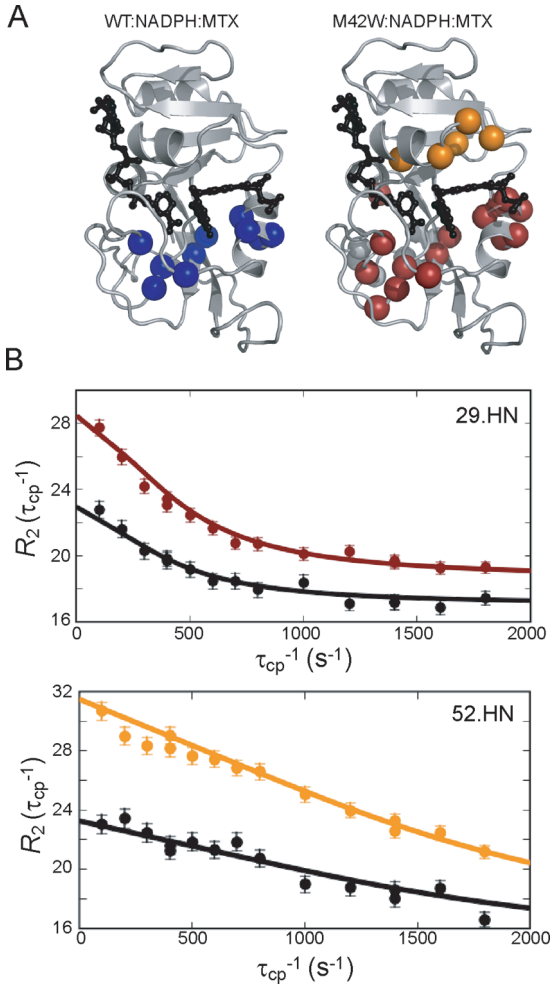

FIGURE 5: Conformational exchange occurs in two distinct regions within M42W-DHFR. (A) The residues that have measurable R_2 dispersion due to conformational exchange are depicted as spheres for the wild-type and M42W-DHFR−NADPH−MTX complexes. For M42W, dispersion curves that are best fitted by k_{ex} values of 4500 and 1100 s^{-1} are colored orange and maroon, respectively. Wild-type dispersion curves were best fitted with a k_{ex} of 430 s^{-1}. (B) Sample relaxation dispersion curves (M42W complex) representative of the exchange in the pABG binding cleft (52.HN) and catalytic core (29.HN) are shown. Colors correlate with the rates described in panel A measured at a ^{1}H spectrometer frequency of 700 MHz. The corresponding data collected at 500 MHz are colored black.

5000 s^{-1} (Figure 5B). These two groups also localize into distinct areas of the protein: the catalytic core and the pABG binding cleft, respectively. These data were fit assuming one or two "global" k_{ex} values. The Bayesion information criterion (BIC), a statistical method used for model selection (*36*), indicates the two-k_{ex} model is appropriate for the M42W−NADPH−MTX complex and fits the data better than a single k_{ex} value, or even using individual (local) k_{ex} values for each R_2 dispersion curve. These results are summarized in Table S3 of the Supporting Information.

The conformational dynamics within the catalytic core of M42W-DHFR appears to be slightly faster than in the wild-type ternary complex. Global catalytic core k_{ex} values were determined to be 430 ± 150 (*17*) and 1200 ± 130 s^{-1} for wild-type and mutant complexes, respectively. This faster rate in the mutant protein is consistent with the observation that residues 14 and 22 display measurable exchange curves, whereas in the wild-type protein, those resonances were too broad to accurately measure. The population of the excited state for both M42W-DHFR and the wild-type protein complex is 2%. It should be noted that, similar to the WT ternary complex (*17*), the Met20 loop does not appear to be switching to the occluded state on the basis of the flat dispersion profile of G121, in addition to $\Delta\omega$ values in Met20 loop residues that are different from those expected for the closed-to-occluded transition.

As discussed above, the exchange rate in the region above the pABG binding cleft (orange spheres in Figure 5) appears to be independent of the conformational switching in the catalytic core of M42W-DHFR. The dispersion curves were best fitted by a global exchange rate k_{ex} of 4500 ± 950 and an excited state population of 3%. Kinetic studies indicate M42W changes the rate of ligand binding and release (*8*, *9*). Below, we discuss the switching rates observed here in comparison to those of product release.

DISCUSSION

Intramolecular Communication in DHFR. Fast motions on the pico- to nanosecond time scale arise from thermal fluctuations within a single, so-called ground state conformational ensemble. As shown using RDC analysis, the structure of M42W-DHFR in complex with MTX and NADPH adopts a closed conformation. In essence, the ground states of WT and M42W-DHFR−NADPH−MTX complexes are structurally identical, and therefore, any pico- to nanosecond dynamical changes are indicative of altered motion without change in the conformational ensemble. While the structure is conserved, the pico- to nanosecond dynamics change throughout M42W-DHFR (Figure 6 and Figure S1 of the Supporting Information).

As shown in Figure 2, the backbone pico- to nanosecond dynamics of G51 and R57 become more flexible. Both residues are located in the MTX (and dihydrofolate) binding pocket, and R57 makes direct contact with the pABG "tail" of MTX (and dihydrofolate). Interestingly, residues 67−69 in the adenosine binding loop collectively become more flexible upon mutation ($\Delta S^2 \sim -0.2$). Binding MTX to the holoenzyme makes these residues become more rigid (*17*); thus, the adenosine binding loop is dynamically coupled to both the active site and M42. In the loops domain, small but significant changes in backbone dynamics at residue A117 indicate the M42W mutation is "felt" in the F−G loop, a region of the protein that is thermodynamically coupled to M42 (*8*). A larger number of dynamic perturbations are observed at methyl-containing side chains (Figure 3), even at sites far removed from position 42 (Figures 4 and 6). These results are consistent with a "network of dynamically coupled" sites throughout DHFR (*52*).

Theoretical and experimental measurements suggest M42W modulates the rate of hydride transfer in part by changing the dynamics within the DHFR active site on time scales similar to those measured here (*10*, *18*). Consistent with these observations, the data indicate motion within the active site of M42W is measurably different from that in the wild-type protein. Specifically, the side-chain methyl dynamics of residues M16, A19, M20, A26, L28, I94, and V99, in addition to the backbone dynamics of residue R57, are altered. These amino acids compose a majority of the folate binding pocket.

The structural distribution of pico- to nanosecond dynamic perturbation is shown in Figure 6. Clearly, the mutational effects span a large distance. As side-chain dynamics studies become more common, long-range dynamical perturbation due to ligand binding or mutation is becoming a common theme among vastly

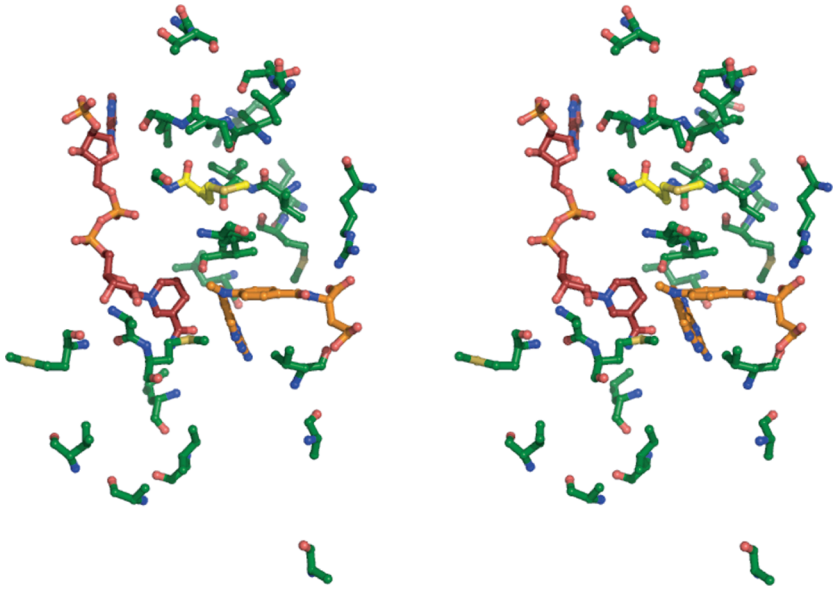

FIGURE 6: Stereoview of the network of dynamical perturbation as a result of the M42W mutation. MTX and NADPH are colored orange and maroon, respectively. Residues that display a significant change in backbone or side chain dynamics are represented by green sticks. M42 is colored yellow.

different proteins, suggesting an underlying dynamic connectivity within the protein scaffold and a potential mechanism for long-range communication (*1*, *50*, *53*−*57*). However, the question of whether these changes follow a recognizable pattern and thus serve as a conduit for transmitting information or if they are random in nature remains. Fuentes and co-workers suggest the dynamical response is not random (*7*). The dynamical response due to ligand binding to a PDZ domain protein was strikingly similar to the network of "thermodynamically coupled" residues identified by Ranganathan and co-workers using sequence-based statistical methods (*5*). In a later study, Fuentes et al. (*51*) discovered the entire "dynamic network" could be modified by mutation of one of the coupled residues. These findings led the authors to suggest that pico- to nanosecond dynamics play a large role in intramolecular signal transduction (*7*). If this phenomenon is common to all proteins and not just to PDZ domains, one would expect to see similar behavior within DHFR.

Thirumalai and co-workers have identified several sites that encompass an "allostery wiring network" within *E. coli* DHFR using both chemical sequence entropy and statistical coupling analysis (*41*). M42 is contained within their wiring network. Therefore, we sought to determine whether the dynamic response observed here and sequence-based networks exhibit significant overlap. As shown in Table 1, the categorical data (e.g., dynamic response or no response) are tabulated in a 2 × 2 matrix for statistical hypothesis testing. The null hypothesis is that no correlation exists between the dynamically perturbed residues (by M42W) and the sequence-derived network. Using Fisher's exact test for hypothesis testing (*39*), we calculate a p of 0.011, leading us to reject the null hypothesis. The p value analysis indicates there is only a 1.1% chance the dynamical changes are not correlated with the allosteric wiring network within DHFR.

Structurally Inferred Analysis of S_{axis}^2: Evidence of a Loss of Correlated Motion in M42W-DHFR. Protein dynamics on the pico- to nanosecond time scale are influenced by local (e.g., residue identity and packing) and nonlocal (e.g., correlated motions) factors (*58*). As discussed above, the distance from the point of mutation is a poor determinant for the change

Table 1: Contingency Table Showing a Correlation between ΔS_{axis}^2 and the DHFR Allostery Wiring Network[a]

	significant ΔS_{axis}^2	insignificant ΔS_{axis}^2	total
in network	12	4	16
not in network	9	19	28
total	21	23	44

[a]Numbers in the table are the number of occurrences. The p value calculated using Fisher's exact test (*39*) 0.011, indicating these occurrences are correlated. See ref *41*.

in S_{axis}^2, and the pattern of perturbation is not random. Here, we seek to illuminate the contribution that local (or nonlocal) interactions make to side chain dynamics. Brüschweiler and co-workers have developed a model for predicting side chain order parameters that accounts for local packing and amino acid type (*40*). We calculated the theoretical methyl order parameters (S_{model}^2) for the WT DHFR−NADPH−MTX complex (PDB entry 1rx3) and compared them to the wild-type and M42W S_{axis}^2 values (Table 2). In principle, the strength of correlation can be degraded by differences in local structure or the influence of long-range correlated motions on S_{axis}^2, should they exist (*59*). If the order parameter values derive from local factors alone, the wild-type S_{axis}^2 versus S_{model}^2 correlation should be significantly higher than the M42W S_{axis}^2 versus S_{model}^2 correlation because S_{model}^2 was calculated using a wild-type crystal structure (that does not account for changes in packing due to the M42W mutation).

In total, five S_{axis}^2 data sets corresponding to the WT−NADPH (*17*), WT−NADPH−MTX (*17*), WT−NADPH−TMP (*17*), WT−$NADP^+$−folate (*60*), and M42W−NADPH−MTX (this work) complexes were compared to S_{model}^2 values. As shown in Table 2, the four wild-type complexes correlate reasonably well with the calculated values. Surprisingly, the M42W S_{axis}^2 values correlate slightly better with the S_{model}^2 values than do any of the wild-type data sets even though the wild-type structure was used to calculate S_{model}^2. To further examine the nature of the correlation, each data set was separated into S_{axis}^2

Table 2: Correlation between Experimental and Predicted S_{axis}^2 Values

complex	r_{total}[a] (n)[b]	r_{loops}[c] (n)[b]	r_{ad}[d] (n)[b]	p value[e] (%)
M42W−NADPH−MTX	0.80 (72)	0.81 (43)	0.77 (29)	N/A
WT−NADPH−MTX	0.74 (69)	0.82 (39)	0.55 (30)	7.2
WT−NADPH	0.73 (63)	0.80 (36)	0.55 (27)	7.8
WT−NADPH−TMP	0.71 (63)	0.81 (36)	0.55 (27)	7.8
WT−$NADP^+$−folate	0.70 (75)	0.81 (40)	0.48 (35)	3.0

[a]Pearson correlation coefficient between measured and predicted side chain order parameters. [b]n is the number of S_{axis}^2 values. [c]Correlation coefficient between experimental and calculated S_{axis}^2 values in the loops domain. [d]Correlation coefficient between experimental and calculated S_{axis}^2 values for the adenosine binding domain. [e]The p value is calculated by comparing r_{ad}(M42W−NADPH−MTX) to r_{ad}(WT complex) for testing the hypothesis H_0: $r_1 = r_2$, H_a: $r_1 > r_2$.

values representing the loops and adenosine binding subdomains. The correlation between S_{axis}^2 and S_{model}^2 values for the loops domain was nearly identical for each protein complex. However, a large difference in correlation was observed for the adenosine binding subdomain. As indicated by the larger r_{ad} value, S_{axis}^2 values for the adenosine binding subdomain of M42W correlate much better with S_{model}^2 values than those of any wild-type complex. It should be noted that these results are independent of the crystal structure used to calculate the order parameter, as S_{model}^2 values for any closed DHFR structure are nearly identical (data not shown).

To determine whether the change in correlation within the adenosine binding domain is significant, we used Fisher's r to z transform. This method enables measurement of the statistical significance in the difference between two given correlations. For each comparison [e.g., r_{ad}(M42W−NADPH−MTX) vs r_{ad}(WT−NADPH−MTX)], we find between 3 and 8% probability that the difference in agreement between the mutant and wild-type protein could happen by chance (Table 2). Thus, the dynamics within the adenosine binding domain of M42W appear to be predicted better by local factors alone than the corresponding dynamics in the wild-type protein. This suggests that correlated motions (or, more accurately, long-range determinants of side chain motion) are reduced in the adenosine binding domain of the M42W ternary complex, relative to those of the wild type, and that side chain motions are dominated to a greater degree by local structural interactions (*59*).

Our analysis is consistent with high-level molecular dynamics simulations of wild-type and mutant DHFR performed by Brooks and co-workers (*15*), who identified several regions of correlated motion between the loops and adenosine binding subdomains. A mutation analogous to the one studied here (M42F) attenuated the long-range correlation (*15*). We propose M42 serves as a "hub" correlating long-range motion and the mutation severs the network of interactions linking the adenosine binding and loops subdomains.

M42W Modulates Dynamics on the Time Scale of Catalysis and Product Release. In addition to decreasing the rate of hydride transfer, M42W changes the rates of ligand binding and dissociation (*8*). While the "artificial" ternary drug complex is not directly relevant to any of these steps, changes in micro- to millisecond dynamics due to mutation may yield insight into mutant-induced dynamical modulation. R_2 relaxation dispersion experiments measure conformational dynamics on a time scale that is most directly relevant to catalysis and product release. Wright and co-workers have established a link between the rate of exchange measured by NMR and each step in the DHFR catalytic cycle (*3*). Our results show that M42W changes the rate of motion on the micro- to millisecond time scale. We observe two distinct groups of residues that experience R_2 dispersion in M42W-DHFR. Within the catalytic core of the protein, 15 residues exhibit measurable exchange. As discussed above, the fitted exchange rate is slightly faster for the mutant protein. The forward rate (k_1) is equal to $\sim$20 s^{-1} as opposed to 10 s^{-1} in the wild-type protein. In essence, the distal mutation allosterically regulates the conformational exchange within the active site of the protein by lowering the energy barrier between the ground and excited state species. As we have noted before, direct comparison of the chemical shifts in the MTX complex with other DHFR structural states is complicated by the presence of MTX around the exchanging residues (*17*). However, the linear correlation of fitted $\Delta\omega$ values from comparable residues in the M42W and wild-type ternary drug complexes indicates the complexes sample similar conformations in the excited state ($r = 0.93$). While the rate is different, the structural identity of the high-energy state within the wild-type and mutant DHFRs appears to be very similar.

A cluster of five residues lining the pABG binding cleft exhibits exchange on the micro- to millisecond time scale in the mutant protein. The exchange rate is much faster and apparently unrelated to the conformational fluctuation within the catalytic core. The fitted exchange rate (4500 s^{-1}) approaches the exchange regime where the Carver−Richards equation fails to separate p_a and $\Delta\omega$. Nevertheless, a globally fitted value of 3.3 ± 1.2% was obtained as a reasonable estimate of the population of the excited state, from which the forward rate of exchange is determined to be 80−250 s^{-1}. Remarkably, this value correlates with the rate of release of tetrahydrofolate from M42W-DHFR (175 s^{-1}) (*8*). Thus, conformational switching in the pABG binding cleft may promote ejection of tetrahydrofolate from M42W-DHFR. Consistent with this possibility, the switching observed in this region, which lines the pABG binding cleft, corresponds to the same group of residues that show concerted switching in the wild-type product release complex (*3*). Further experiments will be required to examine the exact nature of the relationship between conformational exchange in M42W and the rate of catalytic cycling.

CONCLUSION

In this report, we present evidence from a variety of NMR relaxation data that the M42W mutation alters the dynamics of *E. coli* DHFR. The pandynamic strategy used allowed NMR-detected dynamics to be linked with promotion of hydride transfer and correlated motions on the pico- to nanosecond time scale, as well as concerted switching to excited conformational states and product release on the micro- to millisecond time scale. The M42W mutation redistributes conformational dynamics, altering motion in the active site and in regions of the protein that are known to be linked to catalysis. The data also indicate nonlocal structural factors play a larger role in the side chain dynamics of the wild-type protein than in the mutant. This observation is consistent with recent findings that suggest side chain dynamics are in part influenced by networks of correlated motions (*59*). The mutation may suppress these highly evolved correlated motions in DHFR. M42W increases the rate of micro- to millisecond exchange in the core of DHFR and introduces a second faster exchange event on the adenosine binding subdomain. It is intriguing to note that the "fast" millisecond motion

occurs on the same time scale as THF release, providing additional support to the hypothesis that dynamics are important for modulating DHFR product release (*3*). We propose M42 acts as a dynamic hub in DHFR, coordinating motion on multiple time scales. Disrupting these highly evolved dynamic interactions may be an effective method of allosterically modulating protein function.

ACKNOWLEDGMENT

We thank Drs. Karl Koshlap (University of North Carolina Eshelman School of Pharmacy NMR Laboratory) and Greg Young (University of North Carolina Biomolecular NMR Facility) for their technical assistance and members of the Lee Laboratory for invaluable discussion.

SUPPORTING INFORMATION AVAILABLE

A figure showing every residue of DHFR in addition to those dynamically perturbed by M42W, backbone and side-chain order parameters, and fitted relaxation dispersion rates. This material is available free of charge via the Internet at http://pubs.acs.org.

REFERENCES

1. Lee, A. L., Kinnear, S. A., and Wand, A. J. (2000) Redistribution and loss of side chain entropy upon formation of a calmodulin-peptide complex. *Nat. Struct. Biol. 7*, 72–77.
2. Eisenmesser, E. Z., Millet, O., Labeikovsky, W., Korzhnev, D. M., Wolf-Watz, M., Bosco, D. A., Skalicky, J. J., Kay, L. E., and Kern, D. (2005) Intrinsic dynamics of an enzyme underlies catalysis. *Nature 438*, 117–121.
3. Boehr, D. D., McElheny, D., Dyson, H. J., and Wright, P. E. (2006) The dynamic energy landscape of dihydrofolate reductase catalysis. *Science 313*, 1638–1642.
4. Frederick, K. K., Marlow, M. S., Valentine, K. G., and Wand, A. J. (2007) Conformational entropy in molecular recognition by proteins. *Nature 448*, 325–329.
5. Lockless, S. W., and Ranganathan, R. (1999) Evolutionarily conserved pathways of energetic connectivity in protein families. *Science 286*, 295–299.
6. Mittermaier, A., Davidson, A. R., and Kay, L. E. (2003) Correlation between ^{2}H NMR Side-Chain Order Parameters and Sequence Conservation in Globular Proteins. *J. Am. Chem. Soc. 125*, 9004–9005.
7. Fuentes, E. J., Der, C. J., and Lee, A. L. (2004) Ligand-dependent dynamics and intramolecular signaling in a PDZ domain. *J. Mol. Biol. 335*, 1105–1115.
8. Rajagopalan, P. T., Lutz, S., and Benkovic, S. J. (2002) Coupling interactions of distal residues enhance dihydrofolate reductase catalysis: Mutational effects on hydride transfer rates. *Biochemistry 41*, 12618–12628.
9. Ohmae, E., Fukumizu, Y., Iwakura, M., and Gekko, K. (2005) Effects of mutation at methionine-42 of *Escherichia coli* dihydrofolate reductase on stability and function: Implication of hydrophobic interactions. *J. Biochem. 137*, 643–652.
10. Wong, K. F., Selzer, T., Benkovic, S. J., and Hammes-Schiffer, S. (2005) Impact of distal mutations on the network of coupled motions correlated to hydride transfer in dihydrofolate reductase. *Proc. Natl. Acad. Sci. U.S.A. 102*, 6807–6812.
11. Wang, L., Goodey, N. M., Benkovic, S. J., and Kohen, A. (2006) The role of enzyme dynamics and tunnelling in catalysing hydride transfer: Studies of distal mutants of dihydrofolate reductase. *Philos. Trans. R. Soc. London, Ser. B 361*, 1307–1315.
12. Schnell, J. R., Dyson, H. J., and Wright, P. E. (2004) Structure, dynamics, and catalytic function of dihydrofolate reductase. *Annu. Rev. Biophys. Biomol. Struct. 33*, 119–140.
13. Sawaya, M. R., and Kraut, J. (1997) Loop and subdomain movements in the mechanism of *Escherichia coli* dihydrofolate reductase: Crystallographic evidence. *Biochemistry 36*, 586–603.
14. Boehr, D. D., Dyson, H. J., and Wright, P. E. (2008) Conformational relaxation following hydride transfer plays a limiting role in dihydrofolate reductase catalysis. *Biochemistry 47*, 9227–9233.
15. Rod, T. H., Radkiewicz, J. L., and Brooks, C. L., III (2003) Correlated motion and the effect of distal mutations in dihydrofolate reductase. *Proc. Natl. Acad. Sci. U.S.A. 100*, 6980–6985.
16. Rod, T. H., and Brooks, C. L., III (2003) How dihydrofolate reductase facilitates protonation of dihydrofolate. *J. Am. Chem. Soc. 125*, 8718–8719.
17. Mauldin, R. V., Carroll, M. J., and Lee, A. L. (2009) Dynamic dysfunction in dihydrofolate reductase results from antifolate drug binding: Modulation of dynamics within a structural state. *Structure 17*, 386–394.
18. Watt, E. D., Shimada, H., Kovrigin, E. L., and Loria, J. P. (2007) The mechanism of rate-limiting motions in enzyme function. *Proc. Natl. Acad. Sci. U.S.A. 104*, 11981–11986.
19. Friedland, G. D., Lakomek, N.-A., Griesinger, C., Meiler, J., and Kortemme, T. (2009) A Correspondence Between Solution-State Dynamics of an Individual Protein and the Sequence and Conformational Diversity of its Family. *PLoS Comput. Biol. 5*, No. e1000393.
20. Fierke, C. A., Johnson, K. A., and Benkovic, S. J. (1987) Construction and evaluation of the kinetic scheme associated with dihydrofolate reductase from *Escherichia coli*. *Biochemistry 26*, 4085–4092.
21. Muhandiram, D. R., and Kay, L. E. (1994) Gradient-Enhanced Triple-Resonance Three-Dimensional NMR Experiments with Improved Sensitivity. *J. Magn. Reson., Ser. B 103*, 203.
22. Uhrín, D., Uhrínová, S., Leadbeater, C., Nairn, J., Price, N. C., and Barlow, P. N. (2000) 3D HCCH3-TOCSY for Resonance Assignment of Methyl-Containing Side Chains in ^{13}C-Labeled Proteins. *J. Magn. Reson. 142*, 288.
23. Delaglio, F., Grzesiek, S., Vuister, G. W., Zhu, G., Pfeifer, J., and Bax, A. (1995) Nmrpipe: A Multidimensional Spectral Processing System Based on Unix Pipes. *J. Biomol. NMR 6*, 277–293.
24. Johnson, B. A., and Blevins, R. A. (1994) Nmr View: A Computer-Program for the Visualization and Analysis of Nmr Data. *J. Biomol. NMR 4*, 603–614.
25. Eghbalnia, H. R., Bahrami, A., Wang, L., Assadi, A., and Markley, J. L. (2005) Probabilistic Identification of Spin Systems and their Assignments including Coil-Helix Inference as Output (PISTACHIO). *J. Biomol. NMR 32*, 219–233.
26. Loria, J. P., Rance, M., and Palmer, A. G. (1999) A Relaxation-Compensated Carr-Purcell-Meiboom-Gill Sequence for Characterizing Chemical Exchange by NMR Spectroscopy. *J. Am. Chem. Soc. 121*, 2331–2332.
27. Mulder, F. A., Mittermaier, A., Hon, B., Dahlquist, F. W., and Kay, L. E. (2001) Studying excited states of proteins by NMR spectroscopy. *Nat. Struct. Biol. 8*, 932–935.
28. Kay, L. E., Torchia, D. A., and Bax, A. (1989) Backbone dynamics of proteins as studied by ^{15}N inverse detected heteronuclear NMR spectroscopy: Application to staphylococcal nuclease. *Biochemistry 28*, 8972–8979.
29. Muhandiram, D. R., Yamazaki, T., Sykes, B. D., and Kay, L. E. (1995) Measurement of ^{2}H T1 and T1$_\rho$ Relaxation Times in Uniformly ^{13}C-Labeled and Fractionally ^{2}H-Labeled Proteins in Solution. *J. Am. Chem. Soc. 117*, 11536–11544.
30. Ottiger, M., Delaglio, F., and Bax, A. (1998) Measurement of J and Dipolar Couplings from Simplified Two-Dimensional NMR Spectra. *J. Magn. Reson. 131*, 373.
31. Chou, J. J., Gaemers, S., Howder, B., Louis, J. M., and Bax, A. (2001) A simple apparatus for generating stretched polyacrylamide gels, yielding uniform alignment of proteins and detergent micelles. *J. Biomol. NMR 21*, 377–382.
32. Valafar, H., and Prestegard, J. H. (2004) REDCAT: A residual dipolar coupling analysis tool. *J. Magn. Reson. 167*, 228–241.
33. Lipari, G., and Szabo, A. (1982) Model-free approach to the interpretation of nuclear magnetic resonance relaxation in macromolecules. 2. Analysis of experimental results. *J. Am. Chem. Soc. 104*, 4559–4570.
34. Lee, L. K., Rance, M., Chazin, W. J., and Palmer, A. G. (1997) Rotational diffusion anisotropy of proteins from simultaneous analysis of ^{15}N and ^{13}Cα nuclear spin relaxation. *J. Biomol. NMR 9*, 287.
35. Osborne, M. J., and Wright, P. E. (2001) Anisotropic rotational diffusion in model-free analysis for a ternary DHFR complex. *J. Biomol. NMR 19*, 209–230.
36. d'Auvergne, E. J., and Gooley, P. R. (2003) The use of model selection in the model-free analysis of protein dynamics. *J. Biomol. NMR 25*, 25–39.
37. McElheny, D., Schnell, J. R., Lansing, J. C., Dyson, H. J., and Wright, P. E. (2005) Defining the role of active-site loop fluctuations in dihydrofolate reductase catalysis. *Proc. Natl. Acad. Sci. U.S.A. 102*, 5032–5037.
38. Palmer, A. G., III, Kroenke, C. D., and Loria, J. P. (2001) Nuclear magnetic resonance methods for quantifying microsecond-to-millisecond motions in biological macromolecules. *Methods Enzymol. 339*, 204–238.

39. Fisher, R. A. (1922) On the Interpretation of $l^{\pm 2}$ from Contingency Tables, and the Calculation of P. *J. R. Stat. Soc. 85*, 87.
40. Ming, D., and Bruschweiler, R. (2004) Prediction of methyl-side chain dynamics in proteins. *J. Biomol. NMR 29*, 363–368.
41. Chen, J., Dima, R. I., and Thirumalai, D. (2007) Allosteric communication in dihydrofolate reductase: Signaling network and pathways for closed to occluded transition and back. *J. Mol. Biol. 374*, 250–266.
42. Clarkson, M. W., Gilmore, S. A., Edgell, M. H., and Lee, A. L. (2006) Dynamic coupling and allosteric behavior in a nonallosteric protein. *Biochemistry 45*, 7693–7699.
43. Cornilescu, G., Marquardt, J. L., Ottiger, M., and Bax, A. (1998) Validation of Protein Structure from Anisotropic Carbonyl Chemical Shifts in a Dilute Liquid Crystalline Phase. *J. Am. Chem. Soc. 120*, 6836–6837.
44. Mandel, A. M., Akke, M., and Palmer, A. G., III (1995) Backbone dynamics of *Escherichia coli* ribonuclease HI: Correlations with structure and function in an active enzyme. *J. Mol. Biol. 246*, 144–163.
45. Kneller, J. M., Lu, M., and Bracken, C. (2002) An effective method for the discrimination of motional anisotropy and chemical exchange. *J. Am. Chem. Soc. 124*, 1852–1853.
46. Ohmae, E., Iriyama, K., Ichihara, S., and Gekko, K. (1996) Effects of point mutations at the flexible loop glycine-67 of *Escherichia coli* dihydrofolate reductase on its stability and function. *J. Biochem. 119*, 703–710.
47. Pan, H., Lee, J. C., and Hilser, V. J. (2000) Binding sites in *Escherichia coli* dihydrofolate reductase communicate by modulating the conformational ensemble. *Proc. Natl. Acad. Sci. U.S.A. 97*, 12020–12025.
48. Ohmae, E., Iriyama, K., Ichihara, S., and Gekko, K. (1998) Non-additive effects of double mutations at the flexible loops, glycine-67 and glycine-121, of *Escherichia coli* dihydrofolate reductase on its stability and function. *J. Biochem. 123*, 33–41.
49. Igumenova, T. I., Frederick, K. K., and Wand, A. J. (2006) Characterization of the fast dynamics of protein amino acid side chains using NMR relaxation in solution. *Chem. Rev. 106*, 1672–1699.
50. Krishnan, M., and Smith, J. C. (2009) Response of Small-Scale, Methyl Rotors to Protein−Ligand Association: A Simulation Analysis of Calmodulin−Peptide Binding. *J. Am. Chem. Soc. 131*, 10083–10091.
51. Fuentes, E. J., Gilmore, S. A., Mauldin, R. V., and Lee, A. L. (2006) Evaluation of energetic and dynamic coupling networks in a PDZ domain protein. *J. Mol. Biol. 364*, 337–351.
52. Agarwal, P. K., Billeter, S. R., Rajagopalan, P. T., Benkovic, S. J., and Hammes-Schiffer, S. (2002) Network of coupled promoting motions in enzyme catalysis. *Proc. Natl. Acad. Sci. U.S.A. 99*, 2794–2799.
53. Popovych, N., Sun, S., Ebright, R. H., and Kalodimos, C. G. (2006) Dynamically driven protein allostery. *Nat. Struct. Mol. Biol. 13*, 831–838.
54. Jarymowycz, V. A., and Stone, M. J. (2008) Remote changes in the dynamics of the phosphotyrosine-binding domain of insulin receptor substrate-1 induced by phosphopeptide binding. *Biochemistry 47*, 13371–13382.
55. Igumenova, T. I., Lee, A. L., and Wand, A. J. (2005) Backbone and side chain dynamics of mutant calmodulin-peptide complexes. *Biochemistry 44*, 12627–12639.
56. Cooper, A., and Dryden, D. T. (1984) Allostery without conformational change. A plausible model. *Eur. Biophys. J. 11*, 103–109.
57. Clarkson, M. W., and Lee, A. L. (2004) Long-range dynamic effects of point mutations propagate through side chains in the serine protease inhibitor eglin c. *Biochemistry 43*, 12448–12458.
58. Ichiye, T., and Karplus, M. (1991) Collective motions in proteins: A covariance analysis of atomic fluctuations in molecular dynamics and normal mode simulations. *Proteins 11*, 205–217.
59. Law, A. B., Fuentes, E. J., and Lee, A. L. (2009) Conservation of side-chain dynamics within a protein family. *J. Am. Chem. Soc. 131*, 6322–6323.
60. Schnell, J. R., Dyson, H. J., and Wright, P. E. (2004) Effect of cofactor binding and loop conformation on side chain methyl dynamics in dihydrofolate reductase. *Biochemistry 43*, 374–383.
61. Schumann, F. H., Riepl, H., Maurer, T., Gronwald, W., Neidig, K. P., and Kalbitzer, H. R. (2007) Combined chemical shift changes and amino acid specific chemical shift mapping of protein-protein interactions. *J. Biomol. NMR 39*, 275–289.